Aust. J. Phys., 1987, **40**, 73–87

Quiet Ionospheric Currents and Earth Conductivity Profile Computed from Quiet-time Geomagnetic Field Changes in the Region of Australia

Wallace H. Campbell[A] *and Edward R. Schiffmacher*[B]

[A] U.S. Geological Survey, Denver Federal Center,
Mail Stop 964, P.O. Box 25046, Denver, CO 80225, U.S.A.
[B] 2155 Emerald Rd, Boulder, CO 80302, U.S.A.

Abstract

Equivalent ionospheric source currents representing the quiet-day geomagnetic field variations were established for a half-sector of the Earth that included Australia. The analysis used a spherical harmonic separation of the external and internal fields for the extremely quiet conditions existing in 1965. Month-by-month behaviour of the current system indicated a clockwise vortex source with a maximum of $12{\cdot}8\times10^4$ A in January and a minimum of $4{\cdot}4\times10^4$ A in June. The focus location shifted from about $-32{\cdot}5°$ geomagnetic latitude in summer to about $-30{\cdot}0°$ in winter. The separated external and internal field coefficients were used to estimate the Earth's upper mantle electrical conductivity σ at a depth d from about 250 to 350 km as $\sigma = 0{\cdot}00067\exp(0{\cdot}012d)$ S m^{-1} and from about 350 to 550 km as $\sigma = 0{\cdot}0014\exp(0{\cdot}0088d)$ S m^{-1}.

1. Introduction

The primary purpose of this study is to determine the monthly patterns of ionospheric electric currents that could be responsible for the quiet-time daily changes in geomagnetic surface field observed at the southern half-sector of the Earth that includes Australia. These currents should arise from an E-region dynamo process in the ionosphere when daily thermotidal and wind systems of global scale apply a force on the locally ionised particles in the presence of the Earth's main field. Astronomical factors that change both the driving forces and the ionisation give rise to seasonal changes in current patterns. Fields from these primary electric currents induce secondary currents in the conducting Earth. At the surface observatories, a summation of the source and secondary fields are recorded. A gaussian spherical harmonic analysis (SHA) technique allows separation of the source and induced fields representing their potential functions as two converging series of terms whose coefficients are identified by order m and degree n indices. We will use this SHA separation to create the equivalent external current vortex in the ionospheric region of 100 km to describe the solar quiet-time S_q daily changes in the horizontal (northward H and eastward D) and the vertical (downward Z) component field directions at the Earth's surface. Month-to-month changes in this current and field behaviour will be compared with other continental regions of the Earth.

The secondary purpose of this study is to estimate the general conductivity profile of the upper mantle portion of the Earth in the Australian region. The quiet-condition ionospheric source currents induce a flow of eddy currents within the conducting

0004-9506/87/010073$02.00

Earth's mantle. The fields from the S_q system penetrate beneath the crustal levels to a depth dependent upon the effective wavelength of the source and the conducting properties of the deep Earth. With the S_q field decomposed into spherical harmonic terms, each term can be separately analysed as if it alone were the only active surface response composed of an external source current and an internal induced current. The relative behaviour of the amplitude and phase of the two fields of these currents provides information on the penetration depth and effective conductivity within the study region.

On days of minimum solar–terrestrial disturbances an observatory's magnetic records have a smooth appearance throughout the day. The quiet-field amplitudes and phases change form gradually from month to month and show daily features that are rather predictable from year to year. The S_q currents causing these fields are in the ionosphere at about 100 km above the Earth's surface. They have been shown to consist primarily of two great vortices in the sunlit hemisphere, one flowing counter-clockwise in the northern latitudes, the other flowing clockwise in the southern latitudes. Two selections are necessary to study one of the vortex systems: (i) a selection of very quiet days throughout a year and (ii) a distribution of observations from the equator to the pole in one hemisphere.

The selection of 1965 for the analysis year was made for two reasons. It was a very quiet year of the 11-year solar cycle in which about 85 per cent of the 3-hour geomagnetic activity indices K_p had quiet values less than 3 (in active years about 50 per cent are at this level). International cooperation in that year made a large amount of digitised geomagnetic records available in computer readable form at the World Data Center A. For our analysis of the Australian region, we selected days of 1965 when all eight K_p indices were less than 3. Such selection provided 169 days for the analysis.

For any one day in our study of quiet-time conditions, the ionospheric current system can be considered as fixed with respect to the Sun as the Earth rotates under the system. In this view, an observatory samples the field of this current through 360° of longitude in 24 h. Thus, a latitude distribution of observatories from equatorial to polar regions through Australia can be used to sample the behaviour of S_q. Because of the hemispherical scale of this current system, each observatory record contains some information of the entire current pattern; a high density of observatories is not required. Table 1 and Fig. 1 show the location of observatories selected for this analysis. The distribution is adequate but certainly would have been improved somewhat if records had been available at a site between the latitudes of Port Moresby and Gnangara.

The geographic, dip, and geomagnetic latitude locations are all important to the ionospheric current system. An S_q analysis could be carried out in any one of these three locations. Because a truncated series of spherical harmonic coefficients are to represent the phenomenon, the coordinate system most natural to the currents will give the least error in representation. Geographic latitude and the Sun location largely determine both the ionisation and the thermotidal motion in the ionosphere. However, the tensor conductivity in that atmospheric region is quite sensitive to the Earth's main field direction; thus, the dip latitude of a location is important. A dip latitude system would be better to use than the geographic one except for the fact that the slight, nonlinear characteristic of a dip coordinate system would cause trouble in a conductivity analysis because the computed depths are related to field wavelengths

Table 1. Australian region stations

Name	Code	Latitude (deg.)	E. longitude (deg.)	Geomag. latitude (deg.)
Koror	KR	7·33	134·50	−3·2
Port Moresby	PM	−9·40	147·15	−18·6
Gnangara	GN	−31·78	115·95	−43·2
Toolangi	TO	−37·53	145·47	−46·7
Macquarie Is.	MI	−54·50	158·95	−61·1
Dumont D'Urville	DU	−66·67	140·02	−75·7
Wilkes	WK	−66·25	110·58	−77·70
Vostok	VO	−78·45	106·78	−84·2

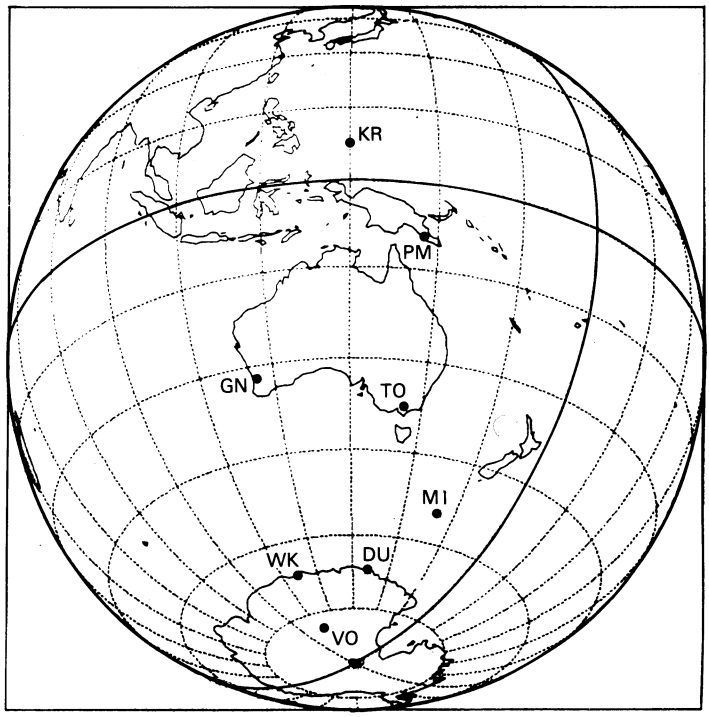

Fig. 1. Geographic location of observatories (Table 1) used in this study.

measured on an equal-angle latitude scale. To avoid any problems of this type, we have selected the geomagnetic-dipole latitude and local-time longitude system as the best representation for this study.

The conductivity determination will depend upon the separated external and internal SHA coefficients computed for the entire analysis region. On first view, such a broad area representation is questionable because considerably different geological environments are encountered with the above station distribution. However, there are three mollifying features that give strength to the analysis. A smoothing over latitude of the Fourier representations for the observed fields (described below) and the smoothing effect of the SHA fitting both tend to remove local shallow conductivity anomaly effects in the results. The field wavelengths of this study should give us conductivity results in the 200–600 km depths; a region where fewer

lateral inhomogeneities are anticipated than closer to the surface. The largest values of the magnetic potential function representing the S_q fields arise near the central region of the current vortex system; we believe that fields near this latitude and longitude dominate the determination of the SHA coefficients and similarly localise the conductivity determinations.

Other studies have used the Australian region magnetic records to understand the S_q current system. Walker (1866) noted that the $S_q(D)$ variations in the Southern Hemisphere were oppositely directed to those of the Northern Hemisphere and found that the daily extreme values at the Hobarton (Tasmania) Observatory often occurred about an hour less than the corresponding extreme values at an equivalent Northern Hemisphere observatory at Toronto (Canada). Matsushita and Maeda (1965) studied S_q for the quiet days of a solar active year dividing the Earth into sectors, one of which represented mainly east Asia, Australia and some Pacific islands (called Zone 2 in their paper) for 4-month data groups representing equinoctial and solstitial seasons. Parkinson (1971) independently analysed a similar period and presented external S_q current patterns for selected hours of Universal Time. Lilley and Parker (1976) found the vertical component of the quiet daily field variations to be larger at the west than at the east coast of Australia and speculated that induction effects were the most likely cause, thereby indicating regional differences in the structure of the continent in addition to a 'coast effect' in the magnetic daily variation. Hibberd (1981) found that the day-to-day variability of $S_q(H)$ at Australian observatories was smaller on the quieter days and could be associated with world-wide causes. From an analysis of quiet-field records taken at a temporary array of stations in Australia, Lilley (1975) found that a representative S_q variation is better obtained by analysing the mean of a number of days rather than transforming the days as a series. We believe that our study is unique in that we will construct an equivalent ionospheric current system for S_q for a limited region centred on Australia and describe its month-to-month changes under exceptionally quiet conditions.

There have been only a few studies of the conductivity profiles that have extended into the upper mantle region beneath Australia. From magnetometer array records of geomagnetic field variations in central and southeast Australia, Woods and Lilley (1979) and Lilley *et al.* (1981*a*, 1981*b*) were able to model the most probable conductivity structure. In central Australia, they found conductivities of about $0{\cdot}01$–$0{\cdot}001$ S m^{-1} starting at about 80 km depth and rising gradually with depth to about 500 km where conductivity rose sharply to about 1–20 S m^{-1} and continued near this value to 600 or 700 km. In south–east Australia, the authors found values of $0{\cdot}01$–$0{\cdot}001$ S m^{-1} from about 50 to 250 km depth where the conductivity rose sharply reaching about 1–100 S m^{-1} at about 350 km. Our study, reported herein, made use of the SHA coefficients of the S_q field representation for the full Australian sector of the Southern Hemisphere to determine a depth profile of equivalent substitute conductors (Schmucker 1970) in the region from about 200 to 600 km. This present study differs from the earlier reports in that a different analysis technique is applied and a general representation of a larger, but overlapping, region is shown.

2. Ionospheric Current Representation

The first step in the analysis was to determine monthly Fourier series representations of the observed quiet variations of the three orthogonal field components for

2·5° geomagnetic latitude increments from the geomagnetic equator to the south geomagnetic pole. Monthly representations of the quiet-field variations were obtained from superposed epoch averages of the selected quiet-day digitisations (typically about 14 each month). For all but one station, these were 2·5 min digitisations from which the lunar tidal effects had been removed by the FAR method (cf. Matsushita and Campbell 1972). For Vostok data we used the hourly value records. The 24, 12, 8 and 6 h Fourier sine and cosine coefficients were determined for each station, component and month from the detrended average records. Next, the seasonal annual and semi-annual Fourier components of 12 (months) detrended daily coefficients were determined. In all, 40 Fourier coefficients sufficed to represent a year's variation of S_q for one field component. Thus, for a geomagnetic component W (for H, D or Z in gammas; 1 gamma $\equiv 10^{-9}$ T), we could reconstruct the field from

$$\Delta W = \sum_{m=1}^{4} \{ C_m \cos(15mt) + S_m \sin(15mt) \}, \tag{1a}$$

where

$$C_m = A_m^0 + \sum_{Q=1}^{2} \{ A_m^{AQ} \cos(30MQ) + B_m^{AQ} \sin(30MQ) \}, \tag{1b}$$

$$S_m = B_m^0 + \sum_{Q=1}^{2} \{ A_m^{BQ} \cos(30MQ) + B_m^{BQ} \sin(30MQ) \}. \tag{1c}$$

Here m is 1–4 for the 24, 12, 8 and 6 h spectral components, respectively; C_m and S_m are the m Fourier cosine and sine coefficients of the daily harmonic changes for a given component, location and time; Q is 1 for annual and 2 for semi-annual; M is the decimal month (0·0 is January 1, and 12·0 is December 31); and t is the local time in decimal hours. The Fourier cosine and sine coefficients of the annual and semi-annual changes are A and B, where mainline letters refer to the annual and semi-annual coefficients, and superscripts refer to the order index coefficients. For the following development, the increment symbol Δ will be dropped.

Each of the 40 coefficients (A_m^0, A_m^{A1}, A_m^{B1}, A_m^{A2}, A_m^{B2}, B_m^0, B_m^{A1}, B_m^{A2}, B_m^{B1}, B_m^{B2} for four m values) representing each of the three directions were arranged by station geomagnetic latitude for smoothing. The coefficient values at Koror (close to the geomagnetic equator) were modified, because of its geographic Northern Hemisphere location, by shifting the annual change 6 months (a change in sign of the annual sine and cosine coefficients) and then the coefficients were taken to represent 0° latitude. Next, a parabolic curve segment was fitted between this equatorial value (as the vertex) and that at the next more southern latitude station. Then linear segments were drawn connecting the values at the remaining observatories, taking Vostok to represent the pole location. Values were read from these curve and line segments at each 2·5° increment. For smoothing, the equatorial value was held to the above measurement; at −2·5°, the assumed value was $\frac{1}{5}$ the sum of 3 times that at the equator and twice the parabola fit value at −2·5°; for all the other 2·5° locations, a five-point running-average method of smoothing was applied to the values obtained from the curve and line segments. Mirror values about the pole were assigned to locations beyond −90° to continue the smoothing to the pole location. At each 2·5° latitude location, values of the smoothed 40 Fourier coefficients for each of the three orthogonal field directions were determined and stored in files.

Fourier cosine and sine coefficients for the monthly analysis spheres were next constructed in this way. The 24, 12, 8 and 6 h components of the daily field variation were taken to correspond to the $(360/m)°$ components of longitudinal field change. For each analysis time sample, S_q field Fourier cosine (c) and sine (s) coefficients, represented by values of X_c^m, X_s^m, Y_c^m, Y_s^m, Z_c^m and Z_s^m, were obtained at each 2·5° Southern Hemisphere latitude location from the C_m and S_m of equation (1) using the smoothed 40 coefficient files. Next a Northern Hemisphere distribution of values was modelled from the study region by assuming that at corresponding latitude locations the Fourier components of H were the same, whereas the D and Z components were oppositely directed; all three field component variations were shifted by 6 months to allow for the seasonal difference. In this way, for each date, coefficients for an analysis sphere were created with field values at all 2·5° latitude increments, pole to pole, as input to the SHA program.

The spherical harmonic analysis coefficients are determined from the global distribution of Fourier coefficients in the following way. We call the 'order' of the computation m (with values 1–4) and the 'degree' of the computation n (with values 1–12). The external cosine and sine coefficients are given by (cf. Matsushita 1967)

$$(a_{ex})_n^m = \{(n+1)a_n^m + c_n^m\}/(2n+1), \tag{2a}$$

$$(b_{ex})_n^m = \{(n+1)b_n^m + d_n^m\}/(2n+1), \tag{2b}$$

and the internal cosine and sine coefficients are

$$(a_{in})_n^m = (na_n^m - c_n^m)/(2n+1), \tag{3a}$$

$$(b_{in})_n^m = (nb_n^m - d_n^m)/(2n+1), \tag{3b}$$

in which a_n^m, b_n^m, c_n^m, d_n^m are computed from

$$a_n^m = \{(2n+1)/4n(n+1)\} \sum_{\theta=0}^{180} \{X_c^m(\mathrm{d}P_n^m/\mathrm{d}\theta)\sin\theta + Y_s^m\, mP_n^m\}\Delta\theta, \tag{4a}$$

$$b_n^m = \{(2n+1)/4n(n+1)\} \sum_{\theta=0}^{180} \{X_s^m(\mathrm{d}P_n^m/\mathrm{d}\theta)\sin\theta - Y_c^m\, mP_n^m\}\Delta\theta, \tag{4b}$$

$$c_n^m = \tfrac{1}{4}(2n+1) \sum_{\theta=0}^{180} Z_c^m\, P_n^m \sin\theta\, \Delta\theta, \tag{4c}$$

$$d_n^m = \tfrac{1}{4}(2n+1) \sum_{\theta=0}^{180} Z_s^m\, P_n^m \sin\theta\, \Delta\theta. \tag{4d}$$

The angle θ is the geomagnetic colatitude and $\Delta\theta$ is the 2·5° step increment of the analysis; P_n^m is the Schmidt normalised associated Legendre function (Parkinson 1983).

The external fields in orthogonal directions with X pointing geomagnetic northward, Y eastward and Z into the Earth may be reconstructed from the external SHA

coefficients as series of Fourier cosine and sine terms of the form

$$\mathscr{X}_{\mathrm{c}}^{m}(\theta) = \sum_{n=m}^{12} (a_{\mathrm{ex}})_n^m (\mathrm{d}P_n^m/\mathrm{d}\theta), \tag{5a}$$

$$\mathscr{X}_{\mathrm{s}}^{m}(\theta) = \sum_{n=m}^{12} (b_{\mathrm{ex}})_n^m (\mathrm{d}P_n^m/\mathrm{d}\theta), \tag{5b}$$

$$\mathscr{Y}_{\mathrm{c}}^{m}(\theta) = -(m/\sin\theta) \sum_{n=m}^{12} (b_{\mathrm{ex}})_n^m P_n^m, \tag{5c}$$

$$\mathscr{Y}_{\mathrm{s}}^{m}(\theta) = (m/\sin\theta) \sum_{n=m}^{12} (a_{\mathrm{ex}})_n^m P_n^m, \tag{5d}$$

$$\mathscr{Z}_{\mathrm{c}}^{m}(\theta) = \sum_{n=m}^{12} n(a_{\mathrm{ex}})_n^m P_n^m, \tag{5e}$$

$$\mathscr{Z}_{\mathrm{s}}^{m}(\theta) = \sum_{n=m}^{12} n(b_{\mathrm{ex}})_n^m P_n^m, \tag{5f}$$

in which $\mathscr{X}_{\mathrm{c}}^{m}$, $\mathscr{Y}_{\mathrm{c}}^{m}$ and $\mathscr{Z}_{\mathrm{c}}^{m}$ are the cosine coefficients of the external orthogonal field components and $\mathscr{X}_{\mathrm{s}}^{m}$, $\mathscr{Y}_{\mathrm{s}}^{m}$ and $\mathscr{Z}_{\mathrm{s}}^{m}$ are the sine coefficients. The 'ex' may be replaced by 'in' in equations (5) when representing the internal horizontal components $\mathscr{X}$ and $\mathscr{Y}$. However, for the vertical internal component, one must use

$$\mathscr{Z}_{\mathrm{c}}^{m}(\theta) = -\sum_{n=m}^{12} (n+1)(a_{\mathrm{in}})_n^m P_n^m, \tag{6a}$$

$$\mathscr{Z}_{\mathrm{s}}^{m}(\theta) = -\sum_{n=m}^{12} (n+1)(b_{\mathrm{in}})_n^m P_n^m. \tag{6b}$$

The sphere over which the analysis has been carried out was created for the necessary boundary conditions of the Gauss method. It is as if the longitudinal pattern of Earth conductivity, responsible for the induced currents, agreed in longitude with that beneath the smoothed Australian region locations and the Northern Hemisphere pattern appropriately matched the southern one. The fields and source currents are thereby given a global distribution. Then, after the SHA coefficients are determined, we consider it to represent only the characteristics within the region of original interest.

Mid-month daily variations of S_{q} (in local time) are shown in Fig. 2 for 10° latitude increments computed from the SHA coefficients with equations (5) and (6). We note the semi-annual variation of the equatorial electrojet (strong H, minimum D and Z component) field. The minimum H variations near $-32°$ signifies the presence of the source current focus. The summer maxima and winter minima are seen at almost all latitudes. The characteristic pre-noon minimum and post-noon maximum in D occurs at most latitude locations throughout the year. The Z components are largest in the polar regions in summer.

A re-creation of the hourly values of fields from the SHA coefficients computed at the original observatory locations was compared with the observed fields. Between

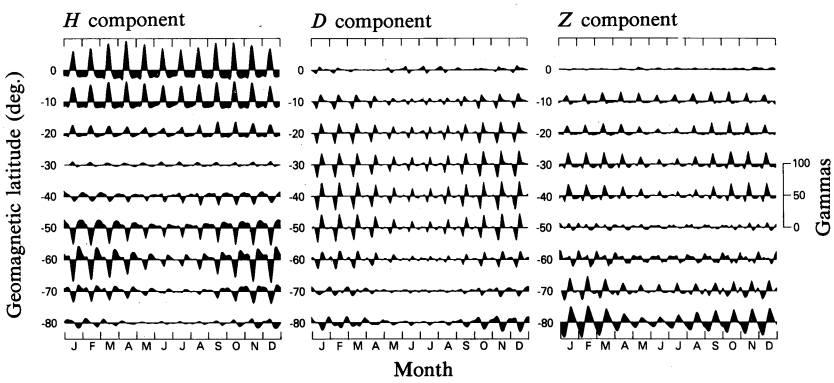

Fig. 2. Daily variations of quiet magnetic field for three orthogonal components D, H and Z in gammas (scale to right). Mid-month variations in local time are illustrated for the analysis months indicated. Values for 10° geomagnetic latitude steps from 0° to −80° are illustrated (scale to left). The amplitudes were computed from the spherical harmonic analysis coefficients representing the regional observations.

the equatorial and auroral latitudes, we found the difference in the computed and observed values to be 10–20 per cent of the observed fields for all three components. Near the equator, there was less than 10 per cent difference. In the polar regions, there was a 25 per cent difference in the two field computations for the three components. The smoothing process carried out in the analysis helped to remove local anomalous behaviour at an observatory location; therefore, we assume that error magnitudes for the SHA analysis process are smaller than these differences.

The equivalent current function $J(\Phi)$ (in A) for hour of the day $\frac{1}{15}\Phi$ is given by the relationship (cf. Matsushita 1967)

$$J(\Phi) = \sum_{m=1}^{4} \sum_{n=m}^{12} \{ U_n^m \cos(m\Phi) + V_n^m \sin(m\Phi) \} P_n^m , \tag{7}$$

in which we use for the external current representation

$$U_n^m = -k\{(2n+1)/(n+1)\}(a_{\mathrm{ex}})_n^m , \tag{8a}$$

$$V_n^m = -k\{(2n+1)/(n+1)\}(b_{\mathrm{ex}})_n^m , \tag{8b}$$

or for the internal representation we take

$$U_n^m = k\{(2n+1)/n\}(a_{\mathrm{in}})_n^m , \tag{9a}$$

$$V_n^m = k\{(2n+1)/n\}(b_{\mathrm{in}})_n^m , \tag{9b}$$

where $k = R/400\pi$ and R is the Earth radius (in m).

Fig. 3 shows the equivalent ionospheric source current stream line contours for the 21st day of each month computed from equations (7) and (8) at 2·5° latitude increments. Each pattern is in local time against latitude coordinates and shows the flow of 10^4 A equivalent current between adjacent contour lines with arrows for the required flow directions. A midnight zero current level was assumed for the computation. We note the annual shift of the current across the equator. From

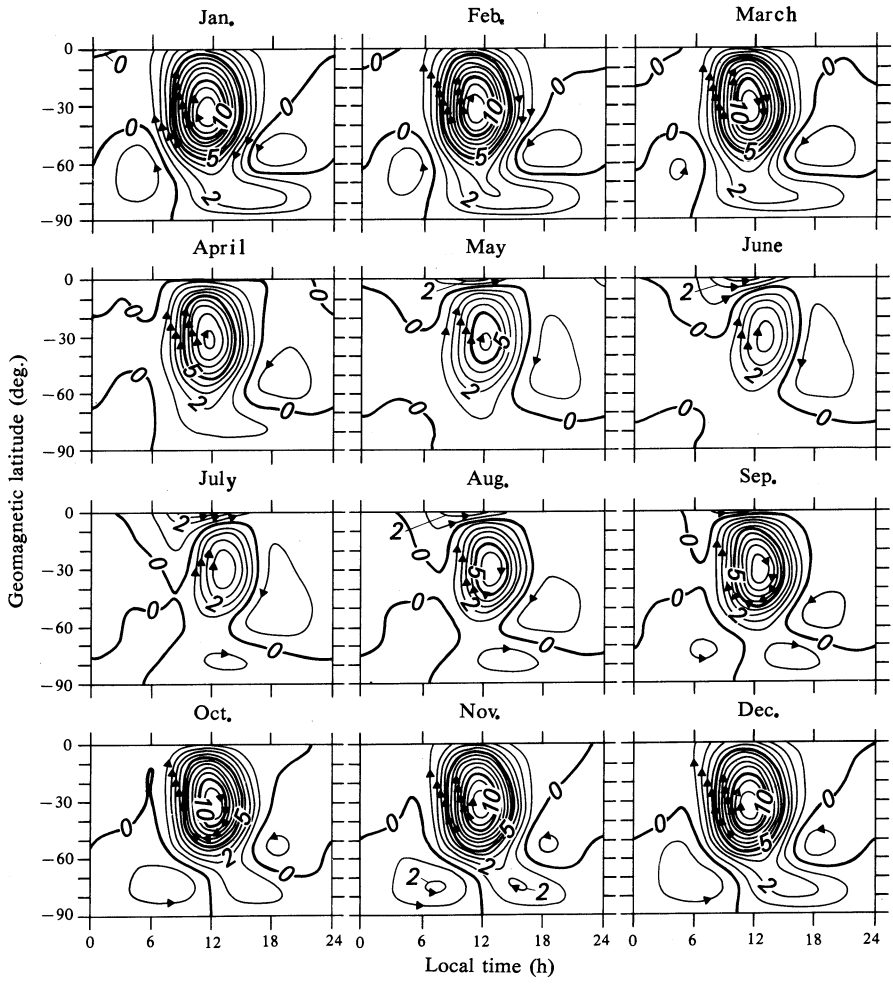

Fig. 3. Month-by-month equivalent ionospheric current representations of the S_q fields for the Australia region study determined from the external spherical harmonic analysis coefficients. A current of 10^4 A flows in the region between contours in the direction of the arrows. A zero level at local midnight was assumed. Each display is in local time against geomagnetic latitude.

Table 2. S_q current characteristics

Month	Current[A]	Lat.[B]	Local time[C]	Month	Current[A]	Lat.[B]	Local time[C]
Jan.	12·8[D]	−32·5	11·4	July	4·8	−30·0	13·2[D]
Feb.	12·7	−32·5[D]	11·2[E]	Aug.	6·8	−30·0[E]	13·0
March	11·7	−32·5	11·4	Sep.	9·7	−30·0	12·4
April	9·2	−32·5	11·6	Oct.	11·9	−32·5	12·2
May	6·2	−32·5	12·2	Nov.	12·7	−32·5	11·8
June	4·4[E]	−32·5	13·0	Dec.	12·7	−32·5	11·6

[A] Total current intensity (10^4 A). [B] Geomagnetic degrees. [C] Focus location hour.
[D] Year's largest value. [E] Year's smallest value.

Table 2 we see that the total current intensity indicated at the focus region attained a maximum of $12{\cdot}8\times10^4$ A in January and a minimum of $4{\cdot}4\times10^4$ A in June. An annual variation of the time of the focus occurrence was observed; it was earliest in February at 11·2 h and latest in July at 13·2 h.

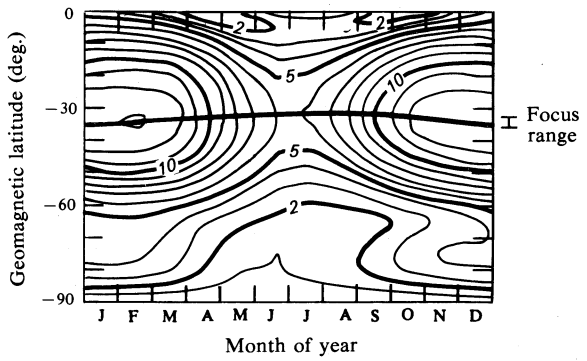

Fig. 4. Contour representation of the daily external current range (10^4 A) displayed for the days of the year (months indicated on x axis) against geomagnetic latitude (y axis). The latitude location of maximum current range for each day provides a trace of the current vortex focus (cf. Fig. 3) through the year. The latitude range of this focus variation is indicated to the right.

The seasonal characteristics of the external current system are better emphasised in another type of plot. For each latitude, the daily range (maximum minus minimum in 24 h) of the external currents was computed at 2·5° latitude increments for the 21st day of each month and contours of this range displayed in a day-of-the-year against geomagnetic latitude coordinate system (Fig. 4). Such a computation is independent of any selection of zero level for the current. The focus movement through the year can be taken as the locus of points of maximum current range computed for each day. The semi-annual variations are noticeable only near the equator; there are current range minima in April and October. The annual variation dominates the entire Australian region pattern; a February maximum and June minimum are clearly evident in the middle latitudes. The locus of the external current vortex focus varies about 2·5° throughout the year; it reaches the most equatorward position of −30·0° in August and most poleward position of about −32·5° in February. At polar locations, the minimum current range occurs at the June solstice.

3. Upper Mantle Conductivity

Schmucker (1970) first introduced the method of profiling the Earth's conductivity with a transfer function utilising the external and internal spherical harmonic coefficients at a given site. This function yielded the depth to equivalent substitute conductors that would produce the observed fields at the Earth's surface. Weidelt *et al.* (1980) and Jones (1983) have demonstrated the equivalence of the Schmucker method to other depth–conductivity profile transformations. Campbell and Anderssen (1983) generalised the form of Schmucker's transfer function C_n^m in the following way:

$$C_n^m = z - \mathrm{i}\,p \tag{10}$$

is a complex number in which real z and imaginary $-p$ parts are given by

$$z = \frac{R}{n(n+1)} \cdot \frac{A_n^m\{n(a_{ex})_n^m-(n+1)(a_{in})_n^m\}+B_n^m\{n(b_{ex})_n^m-(n+1)(b_{in})_n^m\}}{(A_n^m)^2+(B_n^m)^2}, \tag{11a}$$

$$p = \frac{R}{n(n+1)} \cdot \frac{A_n^m\{n(b_{ex})_n^m-(n+1)(b_{in})_n^m\}-B_n^m\{n(a_{ex})_n^m-(n+1)(a_{in})_n^m\}}{(A_n^m)^2+(B_n^m)^2}, \tag{11b}$$

where R (km) is the Earth's radius, z and p are given in km, and the coefficient sums are given by

$$A_n^m = (a_{ex})_n^m+(a_{in})_n^m, \qquad B_n^m = (b_{ex})_n^m+(b_{in})_n^m. \tag{12}$$

For each (n, m) set of coefficients, the depth to the uniform substitute-layer is given by

$$d_{n,m} = z-p\,(\text{km}), \tag{13a}$$

with a substitute layer conductivity of

$$\sigma_{n,m} = 5{\cdot}4\times10^4/m(\pi p)^2\ (\text{S m}^{-1}). \tag{13b}$$

The ratio S_n^m of the internal to external components of the geomagnetic surface field is then

$$S_n^m = u+\text{i}\,v, \tag{14}$$

where

$$u = \frac{(a_{ex})_n^m(a_{in})_n^m+(b_{ex})_n^m(b_{in})_n^m}{\{(a_{ex})_n^m\}^2+\{(b_{ex})_n^m\}^2}, \tag{15a}$$

$$v = \frac{(b_{ex})_n^m(a_{in})_n^m-(a_{ex})_n^m(b_{in})_n^m}{\{(a_{ex})_n^m\}^2+\{(b_{ex})_n^m\}^2}. \tag{15b}$$

The validity of equations (13a) and (13b) is limited by three conditions. The first of these is

$$0^\circ \geqslant \arg(C_n^m) \geqslant -45^\circ; \tag{16}$$

the second condition is

$$80^\circ \geqslant \arg(S_n^m) \geqslant 10{\cdot}5^\circ; \tag{17}$$

the third condition is that the SHA amplitudes (equation 12) not be small. Therefore, we set

$$\{(A_n^m)^2+(B_n^m)^2\}^{0{\cdot}5} \geqslant G_m \tag{18}$$

in which the exclusion factors (in gammas) are $G_1 = 1{\cdot}2$, $G_2 = 0{\cdot}6$, $G_3 = 0{\cdot}4$ and $G_4 = 0{\cdot}3$. The ratio of these amplitudes is about the same as that of the averaged amplitudes of the 24, 12, 8 and 6 h SHA coefficients of the S_q field. These exclusion factors are not a critical determination; when an older G_m selection of 1·5, 1·0, 0·5 and 0·25 was used, there was an insignificant change in the final conductivity profile.

Schmucker's (1970) transfer function was structured for a determination at a particular location with the external and internal SHA coefficients representative of that site. In the present analysis, the SHA coefficients arise from the fitting of a

potential function representation of the smoothed Fourier components of the S_q field obtained in the Australian region and a boundary condition properly modelled in the opposite hemisphere. This potential function has its largest values at the S_q current focus latitudes; and, therefore, this region dominates the SHA coefficients determination. As the focus moves through the year, the principal contributions to the SHA coefficients are obtained from slightly different potential function configurations. The spherical harmonics representing the potential function have $(n-m+1)$ Legendre polynomial oscillations along a great circle of longitude and m Fourier sine wave oscillations along a latitude circle. Potential functions composed of polynomials with odd values of $(n-m)$ represent S_q systems with similar current foci locations in the opposite hemispheres. We use the odd $(n-m)$ terms for the depth analysis to assure more unique latitude sampling of the conductivity–depth determination on any one date.

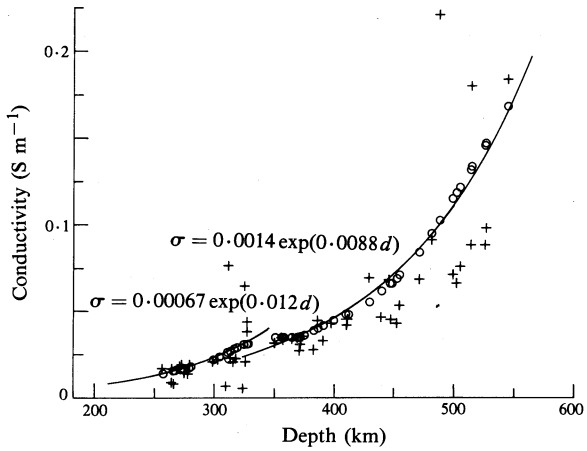

Fig. 5. Values of depth d against conductivity σ. Crosses represent values obtained in the analysis of corresponding external and internal SHA coefficients. Open circles represent the values obtained from the locally weighted regression. The two best fitting exponentials to the regression points are shown with their respective formulation. No values were obtained at depths less than 250 km.

Values of the conductivity σ and depth d for equivalent substitute conductors representing the region were determined with equations (11)–(13) on the 7th and 21st days of each month. An effect of horizontal irregularities in the conductivity represented by the original station distribution was revealed in the computations as the current focus location changed through the year. To accommodate this variation, the year's σ and d values for a given n and m were heavily smoothed using a locally weighted robust regression fitting (Cleveland 1979) of the set. Finally, we made a lightly smoothed locally weighted regression representation of a totality of the above fittings.

The computations provided conductivity values for the region from about 250 to 550 km deep. Fig. 5 shows the resulting conductivity profile together with exponential curves representative of the two sections. The deviation of the computed conductivities from the regression fitting had a mean value of $0{\cdot}016\ \mathrm{S\,m^{-1}}$ with 95% confidence limits at 0·010 and 0·222. A clear break in the conductivity distribution occurs

between about 325 and 375 km. In the shallower region, the conductivity rises from about 0·015 to 0·030 S m^{-1} following an exponential curve similar to

$$\sigma = 0{\cdot}00067 \exp(0{\cdot}012 d) \text{ S m}^{-1}, \tag{19}$$

where σ and d are the conductivity (S m^{-1}) and depth (km) of the computed electrical properties of the study region. In the deeper region, the conductivity rises from about 0·035 to 0·17 S m^{-1} following an exponential similar to

$$\sigma = 0{\cdot}0014 \exp(0{\cdot}0088 d) \text{ S m}^{-1}. \tag{20}$$

4. Discussion

The major features of the quiet-time daily field variations and their ionospheric current representation were quite close to those anticipated from earlier studies. There was a field direction shift for D and Z in the opposite hemispheres. Amplitudes of S_q were largest in summer and smallest in winter. The overall latitude variation of amplitudes had characteristics much like those of the other studied regions (cf. Campbell and Schiffmacher 1985). The current focus was located in the middle latitudes, and the current vortex was oppositely directed to that of the Northern Hemisphere (a result of the oppositely directed main field).

There were a number of unique features of the Australian region current system which differed from those found in other regions (cf. Campbell and Schiffmacher 1985). The ratio of total current magnitudes indicated at the focus in summer and in winter was about 2·9; this was considerably smaller than the value of 6·9 found for the East Asia data set to the north, larger than 2·0 found for North America, and smaller than 4·7 found for Europe. The latitude shift of the S_q focus was only about 2·5°, a value much smaller than 12·5–15·0° found at the Northern Hemisphere sites. The focus was located most poleward in February and most equatorward in August, a parallel to the behaviour of the focus in East Asia. The current focus occurrence times were 0·97 h later than those for East Asia, on the average. This time difference showed a seasonal change, being 1·4 h just before the spring equinox and 0·6 h near the autumn equinox. In correspondence with the summertime atmospheric heating, there was a February maximum of the external current intensity (Fig. 4) quite similar to the post-summer solstice maximum observed for North America but not found in other regions. The mid-latitude annual variation of S_q amplitude in Australia is thought to be typical of the very quiet data samples in 1965; an inclusion of more active data would most likely introduce more semi-annual (equinoxial month) S_q variation similar to most aurorally associated phenomena (cf. Campbell and Matsushita 1982).

The S_q current maxima can be compared with those reported for a more active year. In the analysis by Matsushita and Maeda (1965), Australia and Asia were treated together for the quiet days of 1958. Using 4-month groups of data, they computed the amplitudes over Australia as $18{\cdot}3\times10^4$, $17{\cdot}5\times10^4$ and $12{\cdot}5\times10^4$ A during the December solstice, equinox and June solstice data groups, respectively; the corresponding focus locations were at −38°, −36° and −34° dip latitude. On the average, their reported total current levels were greater than ours by a factor of 1·8 (an expected difference for the comparison of active and quiet years). If we subtract about 5° from their focus locations to obtain the geomagnetic latitude corresponding to the dip, we find that the focus is approximately in the same locations for the

comparable seasons. The small seasonal variability of the focus latitude may be due to the absence of observing sites in the mid-latitudes critical to such determination.

Rayleigh wave seismic studies for the upper mantle beneath Australia by Goncz and Cleary (1976) show a constant velocity level from about 200 to about 400 km and then a distinct increase to another velocity level. For a given range of thermodynamic conditions, the bulk electrical conductivity of the multiphase silicates expected in a given region of the upper mantle is thought to vary exponentially with temperature. The seismic evidence indicates a major change of effective composition phase near 400 km. Therefore, the known increase in temperature with depth would give rise to two exponentials for the conductivity–depth profiles, separated near the 400 km velocity change location. Our results indicate a steady composition above about 250 km, a transition in the effective composition phase from about 325 to 375 km, and a steady composition to at least about 540 km.

Woods and Lilley (1979) and Lilley *et al.* (1981 *a*, 1981 *b*) published deep conductivity estimates for two study regions. Their central Australia results indicated changes near 100–200 km and near 450–600 km and an envelope of possible conductivities that encompass our Fig. 5 values. Their south–east Australia results, which extend to only about 350 km, seem to agree with ours to about 250 km but give a higher conductivity at deeper levels than our values in Fig. 5. We obtained no values at depths less than 250 km.

Our Australian region conductivity profile compares favourably with those of other continental regions (Campbell and Schiffmacher 1986). It is generally similar in values to that found for East Asia and Europe but is lower in conductivity than that found for the corresponding deep levels with the central Asia data.

Acknowledgments

We wish to thank the staff of World Data Center A for Solar Terrestrial Physics for providing magnetograms, data tapes, and some assistance in data manipulation. The work was supported in part by the U.S. Naval Oceanographic Office.

References

Campbell, W. H., and Anderssen, R. S. (1983). *J. Geomagn. Geoelectr.* **35**, 367–82.
Campbell, W. H., and Matsushita, S. (1982). *J. Geophys. Res.* **87**, 5305–8.
Campbell, W. H., and Schiffmacher, E. R. (1985). *J. Geophys. Res.* **90**, 6472–86. (Note correction in **91**, 9023–4, 1986.)
Campbell, W. H., and Schiffmacher, E. R. (1986). *J. Geophys.* **59**, 56–61. (Note correction in **59**, 204–5, 1986.)
Cleveland, W. S. (1979). *J. Am. Stat. Assoc.* **74**, 829–33.
Goncz, J. H., and Cleary, J. R. (1976). *Geophys. J. R. Astron. Soc.* **44**, 507–16.
Hibberd, F. H. (1981). *Aust. J. Phys.* **34**, 81–90.
Jones, A. G. (1983). *J. Geophys.* **53**, 72–3.
Lilley, F. E. M. (1975). *Geophys. J. R. Astron. Soc.* **43**, 1–16.
Lilley, F. E. M., and Parker, R. L. (1976). *Geophys. J. R. Astron. Soc.* **44**, 719–27.
Lilley, F. E. M., Woods, D. V., and Sloane, N. M. (1981 *a*). *Phys. Earth Planet. Inter.* **25**, 419–28.
Lilley, F. E. M., Woods, D. V., and Sloane, N. M. (1981 *b*). *Phys. Earth Planet. Inter.* **25**, 202–9.
Matsushita, S. (1967). *In* 'Physics of Geomagnetic Phenomena' (Eds S. Matsushita and W. H. Campbell), Ch. III-1 (Academic: New York).
Matsushita, S., and Campbell, W. H. (1972). *J. Atmos. Terr. Phys.* **34**, 1187–200.
Matsushita, S., and Maeda, H. (1965). *J. Geophys. Res.* **70**, 2535–58.

Parkinson, W. D. (1971). *Gerlands Beitr. Geophys.* **80**, 199–232.
Parkinson, W. D. (1983). 'Introduction to Geomagnetism' (Scottish Academic Press: Edinburgh).
Schmucker, U. (1970). *J. Geomagn. Geoelectr.* **22**, 9–33.
Walker, E. (1866). 'Terrestrial and Cosmical Magnetism', p. 127 (Deighton Bell: Cambridge).
Weidelt, P., Müller, W., Losecke, W., and Knödel, K. (1980). *In* 'Protokoll über das Kolloquium Elektromagnetische Tiefenforschung' (Eds V. Haak and J. Homilius), pp. 227–30 (Berlin–Hannover).
Woods, D. V., and Lilley, F. E. M. (1979). *J. Geomagn. Geoelectr.* **31**, 449–58.

Manuscript received 23 June, accepted 19 August 1986